JACS
JOURNAL OF THE AMERICAN CHEMICAL SOCIETY

Article

pubs.acs.org/JACS

Exploring Interfacial Events in Gold-Nanocluster-Sensitized Solar Cells: Insights into the Effects of the Cluster Size and Electrolyte on Solar Cell Performance

Muhammad A. Abbas,[†] Tea-Yon Kim,[‡] Sang Uck Lee,[*,§] Yong Soo Kang,[*,‡] and Jin Ho Bang[*,†,§,∥]

[†]Department of Advanced Materials Engineering, Hanyang University, 55 Hanyangdaehak-ro, Sangnok-gu, Ansan, Kyeonggi-do 15588, Republic of Korea

[‡]Department of Energy Engineering, Hanyang University, 222 Wangsimni-ro, Seongdong-gu, Seoul 04763, Republic of Korea

[§]Department of Chemistry and Applied Chemistry, Hanyang University, Ansan 15588, Republic of Korea

[∥]Department of Bionanotechnology, Hanyang University, Ansan 15588, Republic of Korea

Supporting Information

ABSTRACT: Gold nanoclusters (Au NCs) with molecule-like behavior have emerged as a new light harvester in various energy conversion systems. Despite several important strides made recently, efforts toward the utilization of NCs as a light harvester have been primarily restricted to proving their potency and feasibility. In solar cell applications, ground-breaking research with a power conversion efficiency (PCE) of more than 2% has recently been reported. Because of the lack of complete characterization of metal cluster-sensitized solar cells (MCSSCs), however, comprehensive understanding of the interfacial events and limiting factors which dictate their performance remains elusive. In this regard, we provide deep insight into MCSSCs for the first time by performing in-depth electrochemical impedance spectroscopy (EIS) analysis combined with physical characterization and density functional theory (DFT) calculations of Au NCs. In particular, we focused on the effect of the size of the Au NCs and electrolytes on the performance of MCSSCs and reveal that they are significantly influential on important solar cell characteristics such as the light absorption capability, charge injection kinetics, interfacial charge recombination, and charge transport. Besides offering comprehensive insights, this work represents an important stepping stone toward the development of MCSSCs by accomplishing a new PCE record of 3.8%.

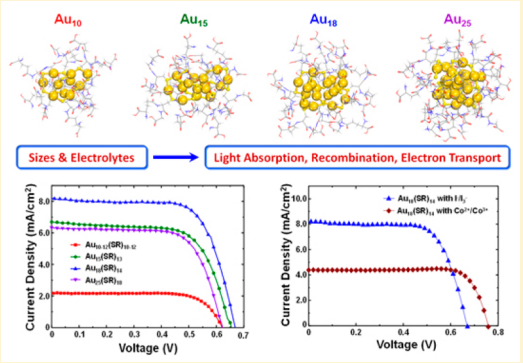

INTRODUCTION

Noble metal NCs (typically sizes of less than 2 nm) have received a great deal of attention due to their distinctive physical properties compared to their larger counterparts.[1] What distinguishes these ultrasmall NCs from larger nanoparticles is the presence of discrete energy levels induced by the quantum confinement effect. In contrast to noble metal nanoparticles where light absorption originates from combined oscillation of charges (i.e., surface plasmons), the absorption of photons occurs via the transition of electrons from ground states to excited states in the NCs. This molecule-like behavior of NCs is responsible for fast-growing interest in exploring NCs in various applications including cellular imaging, biosensors, photocatalysis, and photovoltaics.[2−9] In particular, several important strides have been made in the utilization of NCs in solar light harvesting in recent years. Tatsuma and co-workers reported the first experimental evidence that Au NCs could be used as a visible-light harvester in solar cells whose internal structure is similar to dye-sensitized solar cells (DSSCs) or quantum-dot-sensitized solar cells (QDSSCs).[9,10] Very recently, Kamat and co-workers made an important breakthrough by increasing the photovoltaic performance of Au NC-sensitized solar cells to 2.3% using poly disperse Au_x-glutathione NCs as a sensitizer and a cobalt-based redox couple as an electrolyte.[11] In addition, it has been reported that Ag NCs can also produce a photocurrent when employed as a sensitizer in solar cells,[12] demonstrating the feasibility of using noble metal NCs as a new class of light harvesting antennae. Despite the verified potential of noble metal NCs as a light harvester, research of MCSSCs is still in the embryonic stages. The significantly lower PCE of MCSSCs as compared to their analogues (DSSCs and QDSSCs) has to be further improved. Most of all, a basic understanding of the interfacial events which dictate the performance of this new type of solar cell is required to significantly advance their use. Given that advances of the PCE of DSSCs and QDSSCs have been accompanied by better understanding of these complex internal events over the past few decades, it is of essence to further develop MCSSCs to

Received: November 1, 2015
Published: December 11, 2015

ACS Publications © 2015 American Chemical Society

DOI: 10.1021/jacs.5b11174
J. Am. Chem. Soc. 2016, 138, 390−401

explore the kinetics of the charge transfer processes at interfaces and to determine the limiting factors of the PCE of MCSSCs.

As the first step toward this challenging goal, we paid special attention to the similarities between QDSSCs and MCSSCs. MCSSCs have much more in common with QDSSCs because of the same basic working principle of liquid-junction type solar cells. One of the common aspects is the size-dependent optical and electronic properties of sensitizers. By virtue of various spectroscopic techniques and electrochemical analyses, much information regarding the size-dependent physical properties of QDs has been obtained. Also, the influence of these size-tunable characteristics on the performance of QDSSCs was found to be critical in terms of photoinduced charge injection and charge recombination kinetics, which is well documented in the literature.[13−15] However, little is known about the size dependency of the MCSSC performance. Another important shared feature between these solar cells is the strong dependency of the PCEs on the electrolyte. The early struggles in the development of QDSSCs were primarily attributed to the improper choice of electrolytes that cannot effectively scavenge the holes left in QDs upon photoexcitation. With the use of a polysulfide electrolyte and a highly active electrocatalyst that can couple well with the polysulfide electrolyte, the PCE of QDSSCs has been improved to over 8% in recent years.[16−20] Similar trials and errors have been repeated in the recent development of MCSSCs. As the Kamat group noted, the use of an adequate redox couple (Co^{2+}/Co^{3+}) is critical to extract a steady photocurrent from MCSSCs. However, no attempts to determine the limitations of this redox shuttle or to find a new alternative to obtain an optimal MCSSC configuration have been made yet. Given the significant effects of the QD size and electrolytes on the QDSSC performance, one would think that investigating the impact of these factors on the performance of MCSSCs and elucidating the correlation between them could establish a methodology to boost the PCE of MCSSCs.

In this regard, we performed a systematic investigation of Au NC-sensitized solar cells to elucidate the limiting factors in these solar cells including the light absorption of the sensitizer, charge injection kinetics, charge recombination at the interface, and charge transport. The Au NC-sensitized solar cells were constituted with different-sized Au NCs and electrolytes in this work. Then, they were evaluated by conventional solar cell characterization methods and examined by in-depth EIS analysis. Taking all these results into account together with DFT calculations and physical characterization of the different-sized Au NCs, we obtained a new comprehensive understanding of interfacial events which occur in Au NC-sensitized solar cells for the first time. Our study revealed that the size of the Au NCs *is* substantial in Au NC-sensitized solar cells from the viewpoint of charge injection and recombination kinetics as well as the light absorption capability. Further, we found that the Au NCs are stable enough that they can be operated with the I^-/I^{3-} redox couple and there are no transport limitations in the solar cell performance with this traditional redox mediator. Along with these new insights, this study provides a new milestone in the development of MCSSCs by achieving the highest PCE of 3.8%, which is 1.6 times greater than the highest value previously reported. The detailed results and their implications are discussed herein.

EXPERIMENTAL SECTION

Reagents. L-Glutathione-reduced (98%), cobalt chloride hexahydrate (reagent grade), 2,2′-bipyridyl (99%), ammonium hexafluorophosphate (95%), and nitrosyl tetrafluoroborate (95%) were purchased from Sigma-Aldrich. Hydrogen tetrachloroaurate trihydrate (99.99%) was obtained from Alfa Aesar. $TiCl_4$ was purchased from Junsei Chemical Co. Ltd. The TiO_2 pastes used for the mesoporous layer (Ti-nanoxide, T/SP) and scattering layer (18NR-AO) were purchased from Solaronix and Dyesol-Timo, respectively. The I^-/I_3^- electrolyte (Electrolyte EL-HPE) was purchased from Dyesol-Timo. The EL-HPE is a I^-/I_3^- redox couple based commercial electrolyte, which also contains inorganic iodide salt, organic iodide salt, and pyridine derivative dissolved in a mixture of acetonitrile and valeronitrile.

Synthesis of Au NCs. Au NCs with different sizes $(Au_x(SR)_y$, SR = glutathione) were synthesized as reported previously with slight modifications.[21] Briefly, aqueous solutions of $HAuCl_4$ (20 mM, 12.5 mL) and L-glutathione-reduced (50 mM, 10 mL) were added sequentially to a 500 mL round-bottom flask containing 227.5 mL of deionized water. After stirring for 2 min, the pH of the solution was adjusted using a 1 M NaOH solution. The pH was adjusted to 7, 9, 10, and 11 to synthesize $Au_{10-12}(SR)_{10-12}$, $Au_{15}(SR)_{13}$, $Au_{18}(SR)_{14}$, and $Au_{25}(SR)_{18}$, respectively. Note that $Au_{10-12}(SR)_{10-12}$ is a homoleptic cluster having the same number of Au atoms as the glutathione ligands.[22] The resultant solutions were then purged with carbon monoxide (CO) for 4 min at a flow rate of 10 cm^3/min and left under stirring for 24 h. Au NCs were precipitated by mixing the as-synthesized solution with acetonitrile at a 1:3 ratio and centrifuging at 9000 rpm for 10 min. The resultant precipitates were dried in a vacuum oven and stored in the dark for further experiments.

Fabrication of Solar Cells. TiO_2 films (10 μm-thick mesoporous and 10 μm-thick scattering layer) were prepared on cleaned fluorine-doped tin oxide (FTO) glass substrates using a procedure described elsewhere.[23] To prepare the photoanodes, TiO_2 films were sensitized with different-sized Au NCs by dipping in sensitizing solutions for 24 h. The sensitizing solutions were prepared by dispersing Au NCs in water (~2 mg/mL) and adjusting the pH to 4 using a dilute HCl solution. Since the isoelectric point of anatase TiO_2 is 6.89, the pH of sensitizing solution needed to be adjusted below this value in order for the negatively charged carboxylic groups of glutathione to attach onto TiO_2 surface. Lower pH could enhance the adsorption rate, but it could also lead to the full protonation of carboxylic groups (pK_a values of carboxylic groups in reduced glutathione are 3.4 and 2.05),[24,25] which could reduce the adsorption rate and may also cause the agglomeration of Au NCs by hydrogen bonding. Electrolytes were dropped onto Pt-sputtered FTO glass containing a hot-melt ionomer (Surlyn) which was melted at 90 °C for 5 min on the counter electrode prior to cell fabrication. The counter electrode and photoanode were then carefully assembled using steel clips to prepare a sandwich type cell. $Co(bpy)_3(PF_6)_2$ and $Co(bpy)_3(PF_6)_3$ were synthesized using a method described in the literature.[26] To prepare the cobalt-based electrolyte, 0.22 M $Co(bpy)_3(PF_6)_2$, 0.033 M $Co(bpy)_3(PF_6)_3$, 0.1 M $LiClO_4$, and 0.5 M 4-*tert*-butylpyridine were dissolved in acetonitrile.

Characterization. A UV−vis spectrophotometer (SCINCO S-3100) was used to measure the absorption spectra of the Au NCs. A diffuse reflector (SCINCO) was assembled with the spectrophotometer to measure the transmittance of FTO glass and the reflectance of the photoanodes. Photoluminescence measurements were performed using a spectrofluorometer from Horiba Scientific (Nanolog). The excitation wavelength for $Au_{10-12}(SR)_{10-12}$ was 375 nm while for all other nanoclusters, the excitation wavelength was 470 nm. Fluorescence emission lifetime measurements of the Au NCs were carried out using an inverse time-resolved fluorescence microscope (PicoQuant, MicroTime-200) with 470 nm laser excitation. The photocurrent−voltage (J−V) curve was recorded using a Keithley 2400 source meter while the solar cells (active area: 0.188 cm^2) were illuminated under a solar simulator (HAL-320, Asahi Spectra). A standard silicon diode (CS-20, Asahi Spectra) was used to adjust the light intensity of the solar simulator to 1 sun (Air Mass (AM) 1.5G). The incident photon-to-current efficiency (IPCE) was measured using a PV Measurements Inc. system (QEX7). EIS measurements were carried out in the dark (0.1 Hz to 100 kHz, AC amplitude of 10 mV)

DOI: 10.1021/jacs.5b11174
J. Am. Chem. Soc. 2016, 138, 390−401

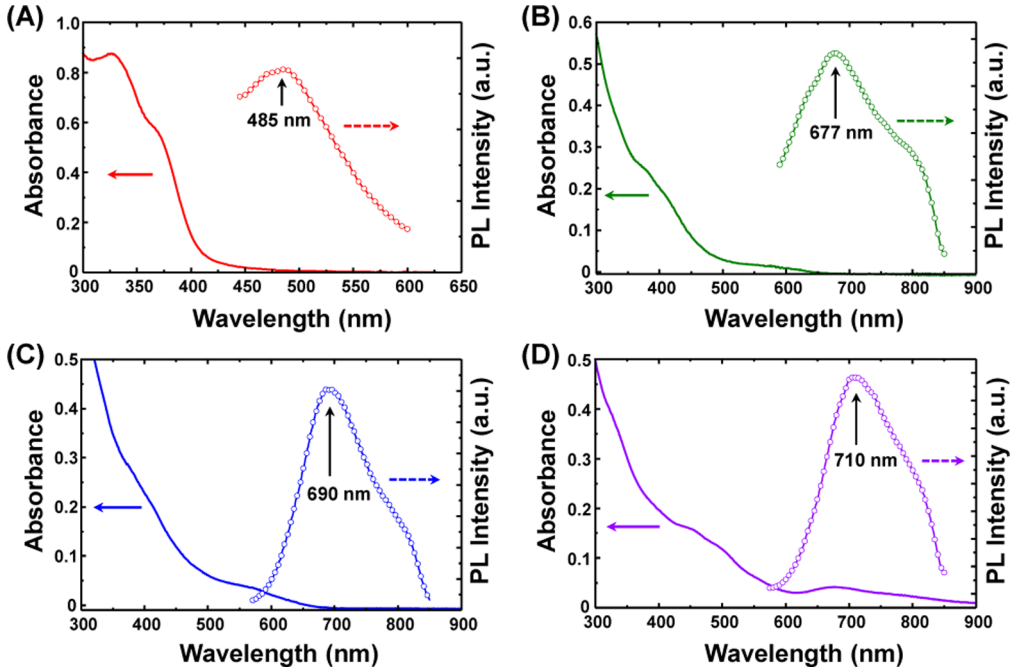

Figure 1. UV−vis absorption and photoluminescence spectra of the (A) $Au_{10-12}(SR)_{10-12}$, (B) $Au_{15}(SR)_{13}$, (C) $Au_{18}(SR)_{14}$, and (D) $Au_{25}(SR)_{18}$ NCs.

using a potentiostat (Autolab, Metrohm). The obtained spectra were analyzed and fitted using a Z-View software with equivalent circuits.

DFT Calculations. The geometries of the neutral (S_0) and cationic states of $Au_{10}(SR)_{10}$, $Au_{15}(SR)_{13}$, $Au_{18}(SR)_{14}$, and $Au_{25}(SR)_{18}$ were optimized by the DFT method using the B3LYP functional.[27] The 6-31G(d,p) basis set[28−30] was used for all atoms except for Au which was treated with LANL2DZ effective core potentials (ECPs) and corresponding basis sets.[31] The adiabatic ionization potential (IP) and optical gap for the energy level diagram of the [TiO_2 electrode]-[Au cluster]-[I_3^-/I^- electrolyte] interface system were calculated. The highest occupied molecular orbital (HOMO) and the lowest unoccupied molecular orbital (LUMO) levels of the energy level diagram correspond to the calculated IP and the difference of the IP and optical gap as follows: HOMO = $E_{cation} - E_{neutral}$ and LUMO = IP − Optical Gap. The electronic transition energies were computed by the time-dependent density functional theory (TD-DFT) method[32] for the optical gap at the same level of the B3LYP/[6-31G-(d,p)+LANL2DZ] theory. The optical gap was determined as the lowest electronic transition energy of the nonzero oscillator strength among the calculated 80 singlet electronic transition energies (300 states used for $Au_{25}(SR)_{18}$). All calculations were carried out using the GAUSSIAN 09 (G09) program. It should be noted that we used Au NC models with a simplified model ligand (methylthio group, $-SCH_3$) instead of the glutathione for the TD-DFT calculations because of the demand of vast calculations. In order to elucidate the effect of the ligands on the calculated results, Au NC models with the full ligand (glutathione) and those with the simplified ligands ($-SCH_3$) were calculated using the SIESTA code, and the resulting calculations were compared.[33−35] A linear combination of localized numerical atomic orbital basis sets was adopted for the valence electrons, and norm-conserving nonlocal pseudopotentials constructed using the Trouiller−Martins scheme[36] were employed for the atomic core. The nonlocal components of the pseudopotentials were expressed in the fully separable form of Kleinman and Bylander.[37,38] The Perdew−Burke−Ernzerhof (PBE) parametrizations of the generalized gradient approximation (GGA) corrections were used for the exchange-correlation potential.[39] The atomic orbital basis set was of single-ζ quality functions (SZ). An auxiliary basis set of a real-space grid was used to expand the electron density for numerical integration. A kinetic energy cutoff of 200 Ry was employed to control the fineness of this mesh. The Brillouin zone was sampled with a k-point grid of (111), according to the Monkhorst−Pack scheme.[40] The atomic positions along with the lattice vectors were optimized by using a conjugate gradient (CG) algorithm, until each component of the stress tensors was reduced below 0.02 GPa and the maximum atomic forces became less than 0.04 eV/Å. The comparison between the Au cluster models with the methylthio ligand and the glutathione ligand is provided in Figure S1 and Table S1 in the Supporting Information. The results show that the effect of ligands on the HOMO level is negligible with the deviations of ∼0.1 eV. Also, the trend of HOMO energy levels changing with the size of Au NCs is similar to that obtained by the G09 calculations at the B3LYP/6-31+G** level of theory. Given the higher accuracy of the TD-DFT formalism, our TD-DFT calculation using the simple model ligand can provide us with reliable energy levels for our discussion.

RESULTS AND DISCUSSION

1. Optical Properties and Electronic Structures of Au NCs with Different Sizes. Since the physical properties of Au NCs are heavily dependent on their size, it is of great importance to investigate the size-dependent optical properties of Au NCs and their influence on the solar cell performance. For this purpose, precise control of the NC size by manipulating the growth kinetics during the reduction of the Au precursor (Au^+-thiolate complexes in many cases) is indispensable. A recent synthesis route developed by Xie and co-workers offers a facile way to delicately control the reduction kinetics by varying the pH, thus allowing the preparation of four different-sized NCs ($Au_{10-12}(SR)_{10-12}$, $Au_{15}(SR)_{13}$, $Au_{18}(SR)_{14}$, and $Au_{25}(SR)_{18}$) on a fairly large scale.[21] The use of glutathione as a thiolate ligand is beneficial in our study because its electron donating groups can suppress self-recombination within the NCs and the two carboxylic groups can play the role as an anchor for the adsorption of Au NCs onto the TiO_2 surface.[9,41] Depending on the pH of the reaction solution, distinctive colors appeared after the reaction, which is indicative of the successful tailoring of Au sizes using this method. Figure 1 shows the absorption and photoemission spectra of all four NCs (detailed characterization of these Au

DOI: 10.1021/jacs.5b11174
J. Am. Chem. Soc. 2016, 138, 390−401

NCs is provided in the previous report).[21] The UV−vis spectra of the as-synthesized Au NCs are well matched with those of $Au_{10-12}(SR)_{10-12}$, $Au_{15}(SR)_{13}$, $Au_{18}(SR)_{14}$, and $Au_{25}(SR)_{18}$ in the literature.[21,22] As anticipated from the quantum confinement effect, the absorption onset of Au NCs becomes red-shifted with increasing size. $Au_{10-12}(SR)_{10-12}$ mostly absorbs in the UV region and its absorption onset lies at ∼450 nm. $Au_{15}(SR)_{13}$ and $Au_{18}(SR)_{14}$ absorb in the visible light region until 700 and 800 nm, respectively. The absorption of $Au_{25}(SR)_{18}$ is the strongest among the four NCs. It absorbs strongly in the visible light region and the absorption onset lies in the near-infrared region down to ∼900 nm. All of the Au NCs also showed photoluminescence, the peaks of which shifted toward the red-region with increasing size where the photoluminescence of the four NCs peaked at 485, 677, 690, and 710 nm, respectively. In the case of $Au_{15}(SR)_{13}$, $Au_{18}(SR)_{14}$, and $Au_{25}(SR)_{18}$, a broad emission peak at ∼800 nm accompanied the main peaks. These emission characteristics coincide with a previous report on glutathione-stabilized Au NCs prepared by the CO reduction method.[42] It is also worth noting that the photoemissions in $Au_{10-12}(SR)_{10-12}$ and $Au_{25}(SR)_{18}$ were the weakest while $Au_{18}(SR)_{14}$ showed the strongest photoemission (Figure S2). This observation is consistent with the fluorescence decay measurements shown in Figure 2. All of the Au NCs exhibited multiexponential decay

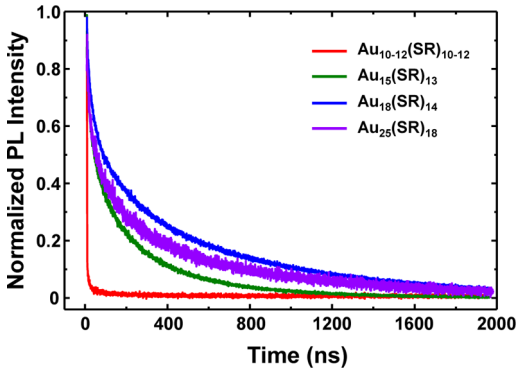

Figure 2. Fluorescence decay curves of the Au NCs.

behavior, each trace of which was fitted with three exponential kinetics (Table 1). $Au_{18}(SR)_{14}$ showed the longest lifetime among them with an average lifetime of 687 ns, which echoes the highest relative photoluminescence intensity. The long lifetime components are dominant over the short-lived components in all of the Au NCs, implying that the ligand-to-metal charge transfer mechanism is primarily responsible for the photoemission. This such long-lived excited state can offer photoinduced electron transfer when Au NCs are coupled with other semiconductors (or dyes) in the form of a type-II junction, which was demonstrated earlier by the Kamat group.[11,22,43] This photoinduced electron transfer process was also proved in our experiments, where gradual emission quenching occurred upon adding TiO_2 colloids into the Au NC suspension (Figure S3).

Despite the proven feasibility of Au NCs as a sensitizer, little is known about the photoinduced electron transfer kinetics. In comparison to QD−TiO_2 couples (e.g., CdSe−TiO_2), where band edges in the QDs are a primary reservoir for excited electrons, the photoexcited electrons in the Au NCs are readily stabilized at a lower relaxed energy state.[11] This results in long-lived excited states in the Au NCs, as observed in both previous reports and our results. Given this difference and the very limited information on the electronic structure of Au NCs, attaining insight into the variation of the electronic structure of Au NCs with different sizes (in particular, HOMO−LUMO positions) is of great importance in order to take a step forward in understanding of the veiled photoinduced electron transfer process. In this regard, TD-DFT calculations were carried out to determine the HOMO−LUMO levels of each Au NC sample. The details of the computations are provided in Table S2−S7 and Figure S4−S7 in the Supporting Information. The simulated UV−vis absorption spectra are presented in Figure 3A (see the energy states constituting the simulated spectra in Table 2 and Figure S4−S7), which bear a close resemblance to those obtained from the experimental measurements shown in Figure 1. The energy diagram of the Au NCs estimated from the theoretical calculations is displayed in Figure 3B and the detailed information is summarized in Table S7. The HOMO−LUMO levels of TiO_2 and the redox potential of electrolytes obtained from the literature are presented along with those of Au NCs.[44,45] When compared with other reports where the HOMO−LUMO levels of glutathione-stabilized Au NCs were experimentally determined, our calculations yielded closely matched energy levels.[9,10] These resemblances along with the close match of the UV−vis absorption spectra ensure the validity and reliability of our TD-DFT calculations. On the basis of this energy diagram, one could conclude that the photoinduced electron transfer from the Au NCs to TiO_2 is feasible, regardless of their size. In addition, the redox potentials of electrolytes are favorable for hole scavenging and hence, the Au NCs could be regenerated without degradation upon photoexcitation. This inference suggests that all of the Au NCs could work as sensitizers in TiO_2-based solar cells. Given the small energy offsets in the case of $Au_{25}(SR)_{18}$, however, we presumed that it might suffer from slower electron injection and retarded regeneration, which will be discussed later in conjunction with the trend of the short-circuit current density.

2. Size-Dependent Solar Cell Performance. Liquid-junction solar cells sensitized with the Au NCs were evaluated to elucidate the influence of their size-dependent photophysical properties on the performance of Au NC-sensitized solar cells. The $J-V$ characteristics and IPCE spectra are presented in Figure 4A and 4B ($J-V$ characteristics under dark condition are shown in Figure S8), respectively, and the solar cell parameters

Table 1. Fluorescence Emission Lifetime Components of the Au NCs[a]

Au NC	a_1	τ_1 (ns)	a_2	τ_2 (ns)	a_3	τ_3 (ns)	$\langle\tau\rangle$ (ns)	χ^2
$Au_{10-12}(SR)_{10-12}$	0.184	0.89	0.205	15.2	0.610	181.9	114.3	1.05
$Au_{15}(SR)_{13}$	0.032	14.36	0.259	121.9	0.709	408.4	321.8	1.11
$Au_{18}(SR)_{14}$	0.019	21.9	0.127	168.8	0.853	779.0	686.6	1.04
$Au_{25}(SR)_{18}$	0.016	14.9	0.163	132.0	0.820	702.7	597.8	0.99

[a]The decay traces in Figure 2 were analyzed using the following equation: $F(t) = a_1e^{-kt1} + a_2e^{-kt2} + a_3e^{-kt3}$.

DOI: 10.1021/jacs.5b11174
J. Am. Chem. Soc. 2016, 138, 390−401

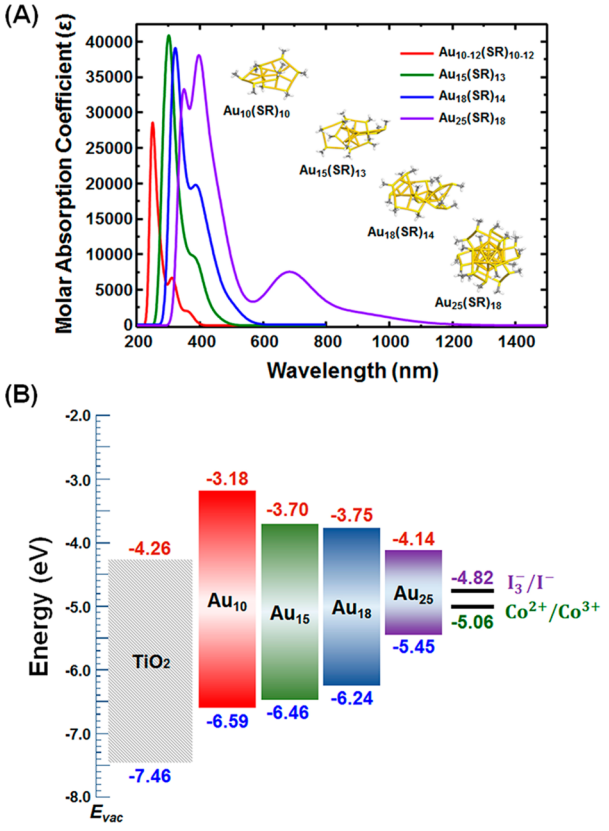

Figure 3. (A) Simulated UV−vis spectra of Au NCs obtained from TD-DFT calculations (inset: structures of the Au NCs used for the calculations) and (B) energy diagrams of the Au NC-sensitized solar cells. The HOMO−LUMO levels of Au NCs were calculated using TD-DFT calculations, the details of which are provided in the Supporting Information. The energy position of TiO_2 and the electrolyte redox levels were obtained from the literature (refs 44 and 45).

are compared in Figure 4C and Table 3. All of the Au NC-sensitized solar cells showed the open-circuit voltages (V_{OC}) of 0.6−0.7 V and the short-circuit currents (J_{SC}) of 2−8 mA/cm^2 with fairly good fill factors (FF) of over 0.7. It is worth noting that our MCSSC with $Au_{18}(SR)_{14}$ was capable of achieving a PCE of 3.8%, which is superior to the previous record reported by the Kamat group (2.36%). The photoaction spectrum of each solar cell resembles the UV−vis absorption spectrum of the corresponding Au NCs (the UV−vis spectra of TiO_2 film sensitized with all four NCs along with digital photographs are also shown in Figure S9), indicating that the photocurrent stemmed from electrons injected from the Au NCs. One of the noticeable observations in the solar cell performance is the trend of the PCE. With increasing size, the PCE increased until $Au_{18}(SR)_{14}$. However, this trend was reversed when the size of the Au NCs further increased from $Au_{18}(SR)_{14}$ to $Au_{25}(SR)_{18}$. Such a trend of the PCE is consistent with the variation of J_{SC} with size (Figure 4C), implying that the photocurrent seems to primarily govern the performance of MCSSCs. The $Au_{18}(SR)_{14}$-sensitized cell showed a 22% higher J_{SC} compared to the cell with the next best candidate, $Au_{15}(SR)_{13}$. The increased J_{SC} of the $Au_{18}(SR)_{14}$-sensitized cell is almost four times higher than that of the $Au_{10-12}(SR)_{10-12}$-sensitized cell. The $Au_{18}(SR)_{14}$-sensitized cell also showed the best V_{OC} among the Au NC-sensitized solar cells. All of the cells showed similar FFs. It is interesting to note that this size dependency observed in our study is consistent with the size-dependent charge transfer characteristics of Au NCs recently investigated by femtosecond transient absorption spectroscopy using methyl viologen as a probe.[22] In this work, $Au_{18}(SR)_{14}$ was also proposed as the best sensitizer with the highest potential due to its favorable electron transfer kinetics and strong visible light harvesting capability.

While the above conventional measurements provided evidence that the size-dependent photophysical properties of Au NCs indeed exert a profound effect on the performance of MCSSCs, comprehensive understanding of the underlying reasons cannot be easily inferred. At quick glance, the PCEs of the Au NC-sensitized solar cells are mainly dictated by the light harvesting capability of Au NCs. In spite of its better light absorption capability, however, the inferior performance of the $Au_{25}(SR)_{18}$-sensitized cell compared to the $Au_{18}(SR)_{14}$-sensitized cell suggests that there are other factors which govern the performance of the Au NC-sensitized solar cells. Given that the performance of liquid-junction solar cells is dictated by a delicate balance among various charge transfer and transport events, seeking better understanding of these processes is critical to obtain deep insight into the size effect. EIS analysis can be a powerful tool to investigate the complicated internal mechanism in MCSSCs. Due to the similarities between MCSSCs and QDSSCs (or DSSCs), we were capable of adapting models well-developed for the analysis of QDSSCs (or DSSCs) for the characterization of the Au NC-sensitized solar cells. Figure 5 shows some important cell parameters obtained from the EIS spectra after fitting to the equivalent circuit developed by Bisquert and co-workers (see Figure S10 and S11 for the EIS spectra and the equivalent circuit).[46−49] Before making a comparison among the different solar cells, the voltage drop due to the series resistance (V_S) and the counter electrode resistance (V_{CE}) of the Au NC-sensitized solar cells was subtracted from the applied bias (V_{app}) to obtain the Fermi voltage ($V_F = V_{app} - V_S - V_{CE}$). V_F is related to the difference of the quasi-Fermi level (E_{Fn}) and equilibrium Fermi level (E_{F0}), which is described by $V_F = (E_{Fn} - E_{F0})/q$, where q is the elementary charge. Figure 5A shows the chemical capacitance (C_μ) as a function of V_F, where C_μ varies with the size of the Au NCs. Since C_μ represents the electron density as a function of the Fermi level, it is linked to the conduction band position of TiO_2 according to the following relationship:

$$C_\mu \propto \exp\left[-\frac{E_{CB} - E_{Fn}}{k_B T}\right] \quad (1)$$

where E_{CB} is the conduction band of TiO_2, E_{Fn} is the quasi-Fermi level, k_B is the Boltzmann constant, and T is the temperature. As seen in both previous reports and our results, the surface modification of TiO_2 by different sensitizers can lead to a subtle change of C_μ (i.e., a different conduction band position of TiO_2) through band alignment.[46,50−53] For fair comparison of the different parameters from the EIS analysis, therefore, all of the Au NC-sensitized solar cells should be considered under a similar number of electrons in the conduction band of TiO_2.[46] To ensure this prerequisite, the voltage scale of C_μ in all cells should be shifted to compensate for the drop of E_{CB} to obtain the equilibrium conduction band position (Figure 5B). Shifting C_μ to the same level ensures the same gap between E_{CB} and E_{Fn}, which eventually leads to a similar number of electrons in the conduction band of TiO_2.

DOI: 10.1021/jacs.5b11174
J. Am. Chem. Soc. 2016, 138, 390−401

Table 2. Contributions of Major Electronic Transitions in First Five Excited States of Different Au NCs[a]

Au NC	state	λ_{calc} (nm)	E (eV)	f_{calc}	major contribution
$Au_{10}(SR)_{10}$	S_1	363.4	3.41	0.0185	HOMO → LUMO (93%)
	S_2	357.2	3.47	0.0070	HOMO → LUMO+1 (93%)
	S_3	328.4	3.78	0.0148	HOMO → LUMO+2 (91%)
	S_4	327.1	3.79	0.0102	HOMO → LUMO+3 (80%)
					HOMO−1 → LUMO (10%)
	S_5	320.6	3.87	0.0008	HOMO → LUMO+4 (45%)
					HOMO−1 → LUMO (41%)
$Au_{15}(SR)_{13}$	S_1	448.5	2.76	0.0132	HOMO → LUMO (99%)
	S_2	413.6	3.00	0.0251	HOMO → LUMO+1 (98%)
	S_3	390.9	3.17	0.0568	HOMO → LUMO+2 (90%)
	S_4	388.1	3.19	0.0267	HOMO−1 → LUMO (82%)
					HOMO−3 → LUMO (5%)
	S_5	376.1	3.30	0.0034	HOMO−2 → LUMO (85%)
					HOMO−3 → LUMO (5%)
$Au_{18}(SR)_{14}$	S_1	498.5	2.49	0.0315	HOMO → LUMO (94%)
	S_2	462.5	2.68	0.0040	HOMO−1 → LUMO (75%)
					HOMO−2 → LUMO (8%)
	S_3	453.1	2.74	0.0129	HOMO → LUMO+1 (48%)
					HOMO−2 → LUMO (41%)
	S_4	450.6	2.75	0.0115	HOMO → LUMO+1 (39%)
					HOMO−2 → LUMO (37%)
	S_5	438.9	2.82	0.0525	HOMO−3 → LUMO (75%)
					HOMO−2 → LUMO (10%)
$Au_{25}(SR)_{18}$	S_1	3394.9	0.37	0.0000	HOMO(β) → LUMO(β) (100%)
	S_2	2665.2	0.47	0.0000	HOMO−1(β) → LUMO(β) (100%)
	S_3	949.9	1.31	0.0016	HOMO−2(β) → LUMO(β) (61%)
					HOMO(α) → LUMO(α) (25%)
	S_4	928.9	1.33	0.0021	HOMO(α) → LUMO+1(α) (48%)
					HOMO−3(β) → LUMO(β) (27%)
					HOMO(α) → LUMO(α) (21%)
	S_5	909.5	1.36	0.0112	HOMO(α) → LUMO(α) (50%)
					HOMO−2(β) → LUMO(β) (33%)

[a] E is the required calculated energy of the photon for the corresponding transition and f_{calc} is the calculated oscillation strength. Note that although the transitions for S_1 and S_2 states in $Au_{25}(SR)_{18}$ are theoretically allowed, their oscillation strength is zero. Hence, they have no contribution in experimental UV−vis spectra.

This condition is referred to as the common equivalent conduction band (V_{ecb}).[46]

The diode equation can be applied to the Au NC-sensitized solar cells to calculate the V_{OC} using the following equation:[54−56]

$$V_{OC} = \frac{k_B T}{q} \ln\left(\frac{\eta \phi_0}{n_0 k_{et}[I_3^-]}\right) \quad (2)$$

where n_0 is the electron density of the conduction band of TiO_2 in the dark, η is the quantum yield of photogenerated electrons, ϕ_0 is the incident photon flux, k_{et} is the rate constant for recombination, and $[I_3^-]$ is the concentration of I_3^- in the electrolyte. Since the $J-V$ measurements were carried out with the same electrolyte and TiO_2 film under the same illumination conditions for all of the cells, one can conclude that the variation of V_{OC} in the cells depending on the NC size depends on two factors, η and k_{et}. V_{OC} is directly proportional to η, which can be correlated with IPCE, suggesting that the $Au_{18}(SR)_{14}$-sensitized cell has the highest η. k_{et} is related to the recombination resistance (R_r). The higher the recombination resistance, the lower the value of k_{et}, which consequently leads to a higher V_{OC}. Figure 5C shows the R_r of all of the Au NC-sensitized solar cells as calculated from the EIS analysis in which the following trend is observed: Au_{15} > Au_{18} > Au_{10-12} > Au_{25}. Although the $Au_{15}(SR)_{13}$-sensitized cell has the highest R_r, it is partly counterbalanced by its lower η, which results in a slightly smaller V_{OC} as compared to the $Au_{18}(SR)_{14}$-sensitized cell. Given the highest V_{OC} in the $Au_{18}(SR)_{14}$-sensitized cell, we speculate that a better balance between R_r and η can be made when $Au_{18}(SR)_{14}$ is used as a light harvester.

The β-recombination model can be used to provide insight into recombination mechanism, in which the recombination in liquid-junction type cells is directly proportional to n^β, where n is the electron density in TiO_2 and β is a constant parameter.[47,57] In this model, R_r as a function of V_F can be given as follows.

$$R_r = R_0' \exp\left(-\frac{q\beta V_F}{k_B T}\right) \quad (3)$$

where R_0' is the pre-exponential factor, or

$$\ln(R_r) = \left(-\frac{q\beta}{k_B T}\right) V_F + \ln(R_0') \quad (4)$$

Eq 4 is a linear relationship. Hence, the slope of the plot of $\ln(R_r)$ *vs* V_F can be used to calculate the β parameter of the cells. Normally, for DSSCs, the β value varies between 0.5 and 0.7. In our case, only the $Au_{18}(SR)_{14}$-sensitized cell gave a β

DOI: 10.1021/jacs.5b11174
J. Am. Chem. Soc. 2016, 138, 390−401

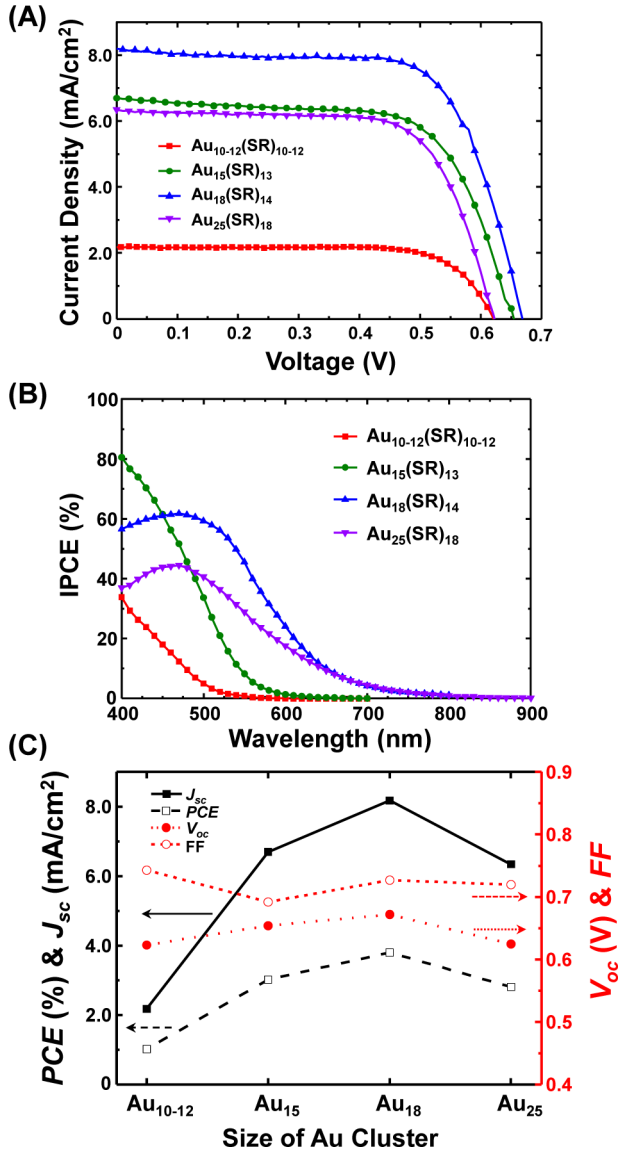

Figure 4. (A) J–V curves, (B) IPCE spectra, and (C) summary of the solar cell parameters of the Au NC-sensitized solar cells.

value close to 0.5, while all other cells showed β values below 0.4 (Figure 5D and Table 3). As Bisquert and co-workers pointed out, this discrepancy has important implications in terms of the recombination mechanism in the Au NC-sensitized solar cells.[46] A β value lower than 0.5 indicates that the Au NCs themselves actively participate in the recombination process. In contrast to DSSCs where recombination with electrolytes is the major recombination process, recombination with the Au NCs is a favored path for the Au NC-sensitized solar cells except for the $Au_{18}(SR)_{14}$-sensitized cell. Because of the more favorable recombination kinetics and better light absorption, $Au_{18}(SR)_{14}$ performed best as a sensitizer for MCSSCs.

All of the Au NC-sensitized solar cells exhibited electron conductivities in TiO_2 (σ_n) on the order of 10^{-3}–10^{-4} $\Omega^{-1}cm^{-1}$ and in the high voltage region, σ_n follows the size of the Au NCs (Figure 5E). However, to gain better understanding of transport limitations in the solar cell performance, examining the ratio of the effective diffusion length to the photoanode thickness (L_n/d) is more insightful, where $L_n = (D_n \times \tau_n)^{0.5}$, D_n is the diffusion coefficient of electron, and τ_n is the electron lifetime (Figure S12).[58] As presented in Figure 5F, the ratios are more than seven at any given V_{ecb} for all of the Au NC-sensitized solar cells. As noted in previous reports, for good performing DSSCs, the ratio must be greater than two to achieve 100% charge collection.[59] This indicates that the performance of Au NC-sensitized solar cells using the I^-/I_3^- redox couple is not limited by electron transport.

In order to obtain more insight into the trend of the J_{SC} of the Au NC-sensitized solar cells, we separated J_{SC} into different components and attempted to determine its limiting factors. J_{SC} is related to the IPCE as follows:

$$J_{SC} = e \int I_0(\lambda) \times \mathrm{IPCE}(\lambda)\, d\lambda \quad (5)$$

where e is the elementary charge, $I_0(\lambda)$ is the solar irradiance spectrum under AM 1.5G conditions, and IPCE(λ) is the incident photon to photocurrent conversion efficiency. IPCE-(λ) can be further deconvoluted into different components using the following equation:[60]

$$\mathrm{IPCE}(\lambda) = \mathrm{LHE}(\lambda) \times \eta_{sep}(\lambda) \times \eta_{coll} \quad (6)$$

where LHE(λ) is the light harvesting efficiency, $\eta_{sep}(\lambda)$ is the charge separation efficiency ($\eta_{sep} = \eta_{inj}(\lambda) \times \eta_{reg}(\lambda)$, where $\eta_{inj}(\lambda)$ is the charge injection efficiency and $\eta_{reg}(\lambda)$ is the regeneration efficiency), and η_{coll} is the collection efficiency of photogenerated charge carriers. In addition to other factors, the LHE(λ) of the photoanode depends on the amount of Au NCs adsorbed onto the TiO_2 film, the thickness and light scattering properties of the photoanode film, and the absorption capability of the adsorbed NCs. If we assume no absorption by the electrolyte inside the pores of the photoanode film and ignore multiple reflections inside the cell, the light harvesting efficiency of the solar cell can be given as follows:[61,62]

$$\mathrm{LHE}(\lambda) = T_{TCO}[1 - R_{PE}(\lambda)](1 - 10^{-\epsilon(\lambda)\Gamma}) \quad (7)$$

where $\varepsilon(\lambda)$ is the molar extinction coefficient of the NCs, Γ is the molar concentration of the NCs per unit area of the TiO_2 film, and $T_{TCO}(\lambda)$ and $R_{PE}(\lambda)$ are the transmittance of FTO

Table 3. Various Parameters for Au NC-Sensitized Solar Cells with Different Sizes

Au NC	J_{SC} (mA/cm^2)	V_{OC} (V)	FF	PCE (%)	ΔE_1[a] (eV)	ΔE_2[b] (eV)	β
$Au_{10-12}(SR)_{10-12}$	2.18	0.632	0.743	1.02	1.08	1.77	0.35
$Au_{15}(SR)_{13}$	6.70	0.654	0.692	3.02	0.56	1.64	0.37
$Au_{18}(SR)_{14}$	8.18	0.672	0.727	3.80	0.51	1.42	0.48
$Au_{25}(SR)_{18}$	6.34	0.625	0.720	2.81	0.12	0.63	0.37
$Au_{18}(SR)_{14}$ with Co^{2+}/Co^{3+}	4.53	0.758	0.809	2.69	0.51	1.18	–

[a]Differences between the LUMO level of the Au NCs and the conduction band of TiO_2. [b]Differences between the redox potential of electrolytes and the HOMO level of the Au NCs.

DOI: 10.1021/jacs.5b11174
J. Am. Chem. Soc. 2016, 138, 390–401

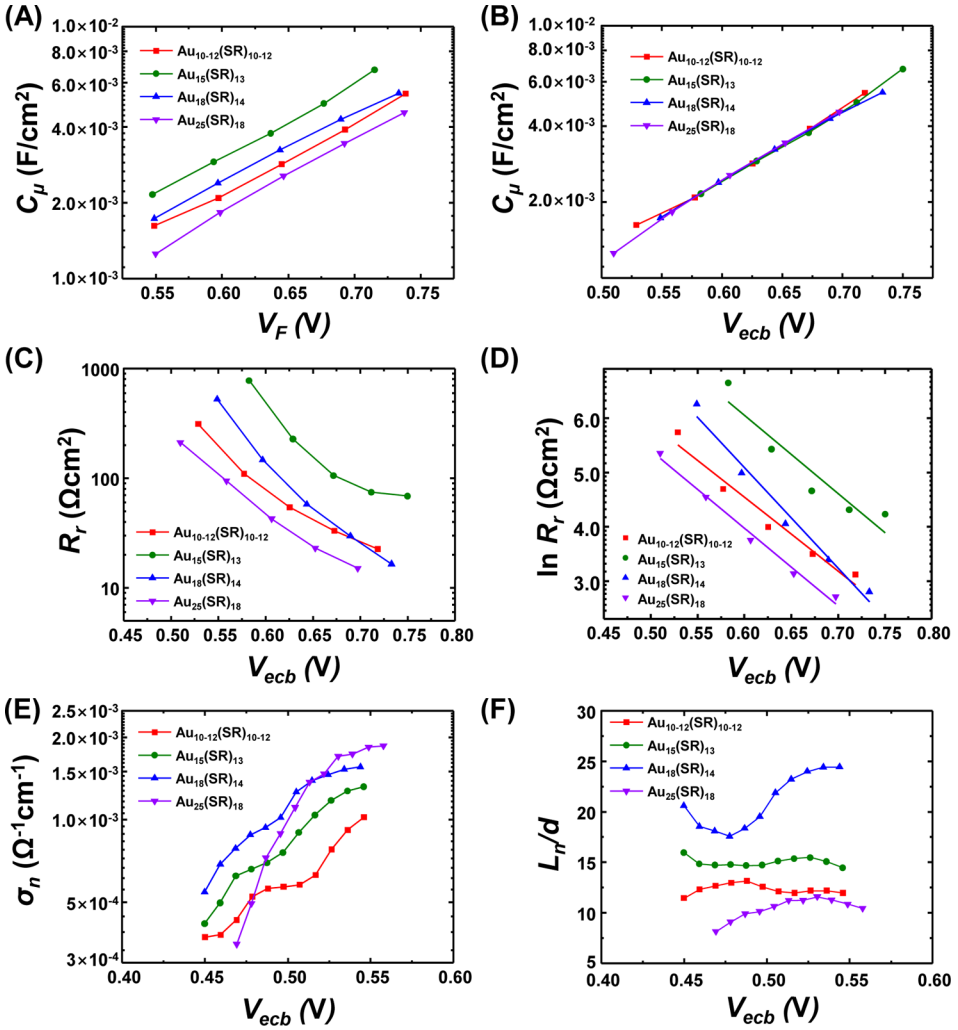

Figure 5. Impedance parameters of the Au NC-sensitized solar cells as determined by EIS analysis. C_μ as a function of (A) V_F and (B) V_{ecb}. (C) R_r, (D) linear fits of eq 4, (E) σ_n, and (F) L_n/d as a function of V_{ecb}.

glass and the reflectance of the photoanode film, respectively. Figure S13A shows the LHE(λ) of the Au NC-sensitized solar cells as calculated using eq 7. Note that the $Au_{10-12}(SR)_{10-12}$-sensitized cell was not analyzed because of very limited absorption under visible light. As expected, with increasing size, LHE(λ) increases because of the better absorption capability of the respective Au NCs. In the liquid-junction solar cells, the limiting processes for η_{coll} are recombination and electron diffusion.[63] The ratio of L_n/d is one of the practical ways to characterize the charge collection performance of the solar cells. In our case, the ratio is larger than 7 in all four cases (Figure 5F), implying that the cells are not transport-limited. Since η_{coll} is almost 100%, with the knowledge of LHE(λ), eq 6 can be used to calculate η_{sep}. Figure S13B shows the η_{sep} values of each cell, where the solar cells sensitized with $Au_{15}(SR)_{13}$ and $Au_{18}(SR)_{14}$ show quite high η_{sep} values but the $Au_{25}(SR)_{18}$-sensitized cell has a very low η_{sep}. The significantly lower η_{sep} in the $Au_{25}(SR)_{18}$-sensitized cell can be rationalized by considering the small energy offsets for $Au_{25}(SR)_{18}$, as depicted in Figure 3B. As noted above, η_{sep} has two components: electron injection (η_{inj}) and NC regeneration (η_{reg}). The driving force for electron injection is the difference between the LUMO level of the Au NCs and the conduction band of TiO_2 (ΔE_1, see the schematic illustration of ΔE_1 in Figure S14).[64] Typically, in the case of DSSCs, ΔE_1 should be more than 0.2 eV for efficient electron injection.[65−69] For the $Au_{25}(SR)_{18}$-sensitized cell, this difference is only 0.12 eV, while ΔE_1 is higher than 0.5 eV for the other cells (Table 3). While the working principles of DSSCs and MCSSCs are not exactly the same, they possess many common features in their operation mechanisms. Care is required when assessing the characteristics of MCSSCs (ΔE_1 and ΔE_2) with respect to the gauge used for the characterization of DSSCs. However, it is rational to compare the relative efficiencies of electron injection and NC regeneration (mostly dictated by the size of Au NCs in our study) with respect to the criteria employed for DSSCs. Judging from the above criteria for efficient electron injection, it is apparent that η_{inj} is substantially lower for the $Au_{25}(SR)_{18}$−TiO_2 couple than for other counterparts. From the viewpoint of regeneration, on the other hand, the energy difference to drive hole scavenging (ΔE_2, see the schematic illustration of ΔE_2 in Figure S14) is not sufficiently large for $Au_{25}(SR)_{18}$. The energy difference between the HOMO level and E_{redox} (ΔE_2) is only 0.63 eV for $Au_{25}(SR)_{18}$, which is substantially smaller than those for other Au NCs (1.4−1.7 eV, Table 3). Given that a ΔE_2 of 0.8−0.9 eV is required for more than 95% regeneration of photoexcited dyes in DSSCs using the I^-/I_3^- electrolyte,[45,70−72] the η_{reg} of the $Au_{25}(SR)_{18}$-sensitized cell is also inferior to those of other

DOI: 10.1021/jacs.5b11174
J. Am. Chem. Soc. 2016, 138, 390−401

cells. Both these unfavorable factors contribute to the notably lower η_{sep} and consequently result in the lower J_{SC} for the $Au_{25}(SR)_{18}$-sensitized cell in spite of its better light absorption capability. Unlike the $Au_{25}(SR)_{18}$-sensitized cell, the J_{SC} value of the $Au_{15}(SR)_{13}$-sensitized cell seems to be primarily restricted by the limited light harvesting capability of $Au_{15}(SR)_{13}$ (i.e., lower LHE(λ)). In the case of the $Au_{18}(SR)_{14}$-sensitized cell, a relatively higher LHE(λ), optimum η_{sep}, and the lowest self-recombination (i.e., the longest fluorescence lifetime) are notably characteristic. We speculate that all of these favorable conditions lead to the highest J_{SC} for the $Au_{18}(SR)_{14}$-sensitized cell.

3. Electrolyte Effect on the Solar Cell Performance. Given the many reports regarding the role of electrolytes on the performance of liquid junction solar cells,[73] the choice of electrolyte that can couple well with Au NCs should be carefully made to maximize the PCE of Au NC-sensitized solar cells. Besides working as an electron donor to regenerate photoexcited Au NCs, the electrolyte is a key player in the solar cell operation in that it can readily participate in the recombination process through back electron transfer from TiO_2 to the electrolyte. Despite the importance, little effort has been made to date to elucidate the influence of electrolytes on the performance of MCSSCs. While several electron donors such as iodide, thiocyanate, triethanolamine, hydroquinone, phenol, and benzyl alcohol were examined in early reports, their compatibility with Au NCs was only briefly investigated.[9,10] The recent monumental record in the PCE of MCSSCs demonstrated by the Kamat group was in fact attributed to the wise choice of electrolyte based on the Co^{2+}/Co^{3+} redox couple.[11] To our surprise, despite our early concerns regarding corrosion, the I^-/I_3^- redox couple successfully works with the Au NCs. As demonstrated above, $Au_{18}(SR)_{14}$ performed the best with the I^-/I_3^- redox couple among the prepared Au NCs, setting a new PCE record of 3.8%. Motivated by this unanticipated success, we compared the iodide- and cobalt-based electrolytes to gain more insight into their characteristics. Figure 6A compares the $J-V$ curves of the $Au_{18}(SR)_{14}$-sensitized cell working with the I^-/I_3^- and $Co(bpy)_3(PF_6)_2$/$Co(bpy)_3(PF_6)_3$ redox couples ($J-V$ curves under dark conditions are shown in Figure S15). As compared to the cell operating with the I^-/I_3^- couple, the J_{SC} of the cell employing the Co^{2+}/Co^{3+}-based electrolyte decreased from 8.18 to 4.53 mA/cm^2. However, the V_{OC} of the Co^{2+}/Co^{3+}-based cell increased from 672 to 758 mV and its FF also improved substantially from 0.73 to 0.81. The overall PEC of the $Au_{18}(SR)_{14}$-sensitized cell was reduced from 3.8% to 2.7% (Table 3) when the $Co(bpy)_3(PF_6)_2/Co(bpy)_3(PF_6)_3$ redox couple was used because of the dramatic decrease of J_{SC}. The IPCE spectra (Figure 6B), where the solar cell with the Co^{2+}/Co^{3+} redox couple shows significantly decreased IPCE values between 400 and 650 nm, echo the decreased J_{SC} observed in the $J-V$ measurements. Although the cobalt complexes have several advantages over the iodide redox couple (e.g., relative inertness, lower light absorption, and ability to tune the redox potential by introducing different ligands or by changing the ratio of Co^{2+} and Co^{3+}),[74−77] their bulky ligands often hinder the effective mass transport of this redox couple through the mesoporous TiO_2 film. As the oxidized species should return to the counter electrode to complete the working mechanism of MCSSCs, this retarded diffusion is likely to reduce the photocurrent produced in the cell. The photocurrent transient measurements in Figure S16 support our hypothesis. With the

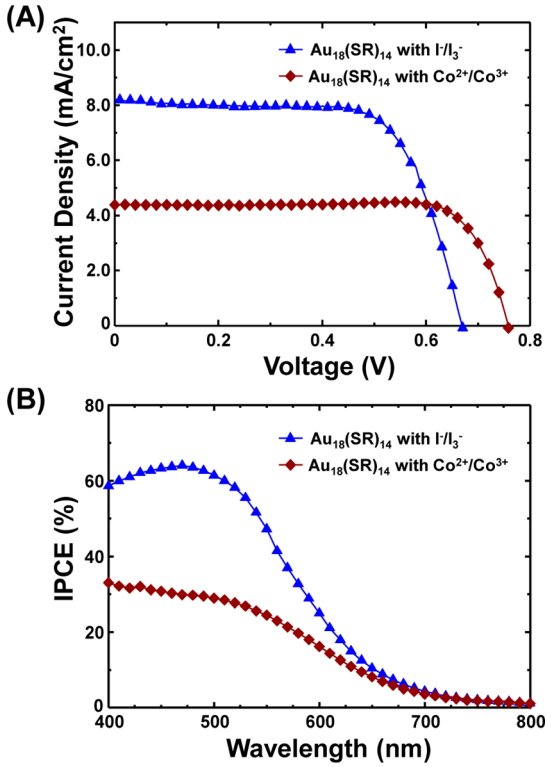

Figure 6. (A) $J-V$ curves and (B) IPCE spectra of $Au_{18}(SR)_{14}$-sensitized solar cells with different electrolytes.

cobalt redox couple, the photocurrent decay over time was more pronounced, which has been previously attributed to the limited mass transport in liquid junction solar cells.[78−80]

The EIS analysis provides more insight into the effect of electrolyte on the performance of Au NC-sensitized solar cells. One of the noticeable features in the EIS analysis is the huge decrease of the C_μ of the solar cell with the cobalt-based electrolyte (Figure 7A), indicating an increase of the conduction band of TiO_2. We define ΔE_C as the displacement in the conduction band of TiO_2 relative to its position when $Au_{18}(SR)_{14}$ is used as a sensitizer with the I^-/I_3^- redox couple. ΔE_C was found to be about −170 mV, which can consequently result in a larger V_{OC} for the solar cell working with the cobalt-based electrolyte. The increased V_{OC} of 86 mV in our $J-V$ measurements indeed reflects such a great discrepancy in the conduction band position. However, the Co^{2+}/Co^{3+}-based cell exhibits a substantially lower recombination resistance (Figure 7B), which inevitably results in the decreased J_{SC}. As discussed earlier, the J_{SC} of solar cells is determined by three different factors (LHE(λ), η_{coll}, and η_{sep}). Since we used the same photoanode for both electrolytes, the LHE(λ) of both cells should be the same. As for η_{sep}, $\eta_{inj}(\lambda)$ and $\eta_{reg}(\lambda)$ are the two major factors dictating the efficiency. $\eta_{inj}(\lambda)$ is related to ΔE_1 while $\eta_{reg}(\lambda)$ is related to ΔE_2. ΔE_1 is the same because the same sensitizer ($Au_{18}(SR)_{14}$) was used for both cells and ΔE_2 for the Co^{2+}/Co^{3+}-based cell (1.18 eV) seems to be large enough for the hole scavenging, given that the required driving force for Ru-based dye regeneration by Co-complexes is typically 0.6−0.7 eV.[45,72,81,82] Thus, one could speculate that J_{SC} is likely to be governed primarily by η_{coll}. Indeed, the solar cell operating with the Co^{2+}/Co^{3+} redox couple showed a very low electron conductivity and much shorter effective diffusion length than the thickness of the photoanode (Figure S17). The

DOI: 10.1021/jacs.5b11174
J. Am. Chem. Soc. 2016, 138, 390−401

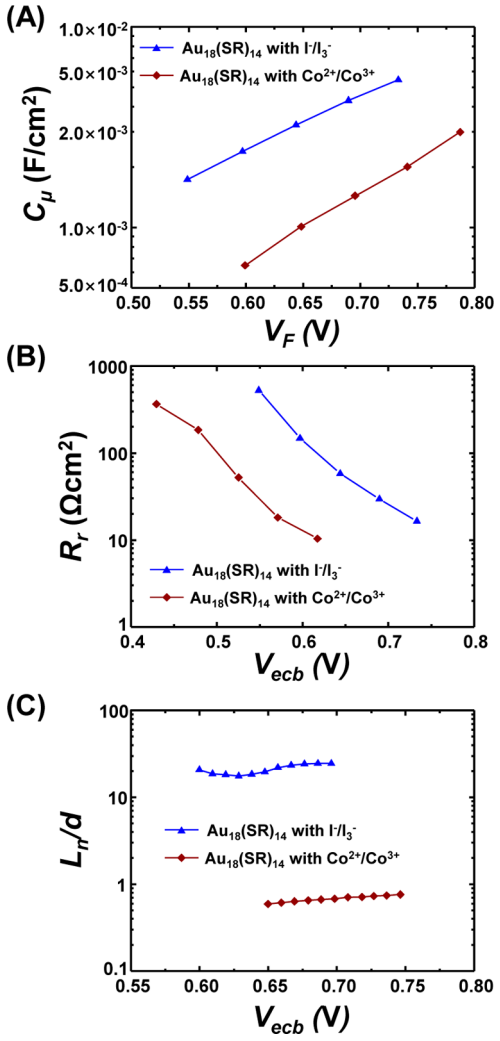

Figure 7. Impedance parameters of $Au_{18}(SR)_{14}$-sensitized solar cells with two different redox couples as determined by EIS analysis. (A) C_μ as a function of V_F, and (B) R_r and (C) L_n/d as a function of V_{ecb}.

resulting L_n/d value for the Co^{2+}/Co^{3+}-based cell is ~0.5 (Figure 7C), which leads to a collection efficiency of ~50%. This is notably different from the cell working with the I^-/I_3^- redox couple ($\eta_{coll} \approx 100\%$). The Co^{2+}/Co^{3+}-based solar cell also showed lower electron lifetimes (Figure S17B), which was further confirmed by the open-circuit voltage decay measurements (Figures S18 and S19).[83] The limited electron transport and lower recombination resistance are the most probable processes responsible for the dramatic decrease of the J_{SC} of the solar cell operating with the Co^{2+}/Co^{3+} redox couple.

CONCLUSIONS

In summary, we provided the first insights into various interfacial events in Au NC-sensitized solar cells and elaborated their size-dependent photovoltaic properties. This study is also the first successful demonstration of the use of the I^-/I_3^- redox couple for Au NC-sensitized solar cells. We found that $Au_{18}(SR)_{14}$ served best as a sensitizer and achieved a new PCE record of 3.8%. According to the EIS analysis, this high PCE is attributed to the relatively good light absorption capability and low recombination rate in the $Au_{18}(SR)_{14}$-sensitized solar cell. Despite its better absorption up to the near-infrared region, $Au_{25}(SR)_{18}$ showed much lower J_{SC} and V_{OC} values, which are linked to the very poor recombination resistance. In contrast, the limited light harvesting capability of $Au_{15}(SR)_{13}$ is mostly responsible for the lower PCE of the $Au_{15}(SR)_{13}$-sensitized solar cell. Our EIS studies revealed that there are no transport limitations for the Au NC-sensitized solar cells when using I^-/I_3^- as the electrolyte. Hence, the recombination resistance and light absorption capability are the main factors in determining the solar cell performance. Solar cells with the cobalt-based electrolyte showed a much lower J_{SC} in spite of the higher V_{OC}, as compared to the cells working with the I^-/I_3^- electrolyte. We found that a significantly lower recombination resistance and a shorter carrier diffusion length are the limiting factors for the Co^{2+}/Co^{3+} redox couple. Our preliminary results, however, suggest that for any long-term use of Au NCs, the Co^{2+}/Co^{3+} redox couple may be the best option as an electrolyte because of its relative inertness (Figure S20). Given that the simple shift from a liquid corrosive electrolyte to a solid-state hole transporter such as 2,2′,7,7′-Tetrakis(*N*,*N*-di-4-methoxyphenylamino)-9,9′-spirobifluorene (spiro-OMeTAD) was the dramatic turning point in the development of perovskite solar cells,[84] we believe that it is essential to develop a suitable hole scavenger that couples well with the Au NCs for future improvements of Au NC-sensitized solar cells.

ASSOCIATED CONTENT

Supporting Information

The Supporting Information is available free of charge on the ACS Publications website at DOI: 10.1021/jacs.5b11174.

Additional experimental data and analysis (PDF)

AUTHOR INFORMATION

Corresponding Authors

*sulee@hanyang.ac.kr
*kangys@hanyang.ac.kr
*jbang@hanyang.ac.kr

Notes

The authors declare no competing financial interest.

ACKNOWLEDGMENTS

This research was supported by grants from the Basic Science Research Program through the National Research Foundation of Korea (NRF) funded by the Ministry of Science, ICT, and Future Planning (NRF-2013R1A1A1008762, NRF-2015R1C1A1A02036670, and 2008-0061891). The DFT calculation study was supported by the Supercomputing Center/Korea Institute of Science and Technology Information with supercomputing resources including technical support (KSC-2015-C1-024). The fluorescence emission lifetime measurements were performed at the Korea Basic Science Institute (KBSI).

REFERENCES

(1) Jin, R. *Nanoscale* **2015**, *7*, 1549−1565.
(2) Zhang, X.-D.; Luo, Z.; Chen, J.; Shen, X.; Song, S.; Sun, Y.; Fan, S.; Fan, F.; Leong, D. T.; Xie, J. *Adv. Mater.* **2014**, *26*, 4565−4568.
(3) Zhang, P.; Yang, X. X.; Wang, Y.; Zhao, N. W.; Xiong, Z. H.; Huang, C. Z. *Nanoscale* **2014**, *6*, 2261−2269.
(4) Xu, Y.; Sherwood, J.; Qin, Y.; Crowley, D.; Bonizzoni, M.; Bao, Y. *Nanoscale* **2014**, *6*, 1515−1524.
(5) Xie, J.; Zheng, Y.; Ying, J. Y. *Chem. Commun.* **2010**, *46*, 961−963.
(6) Xiao, F.-X.; Hung, S.-F.; Miao, J.; Wang, H.-Y.; Yang, H.; Liu, B. *Small* **2015**, *11*, 554−567.

DOI: 10.1021/jacs.5b11174
J. Am. Chem. Soc. 2016, 138, 390−401

(7) Yu, C.; Li, G.; Kumar, S.; Kawasaki, H.; Jin, R. *J. Phys. Chem. Lett.* **2013**, *4*, 2847−2852.
(8) Chen, Y.-S.; Kamat, P. V. *J. Am. Chem. Soc.* **2014**, *136*, 6075−6082.
(9) Sakai, N.; Tatsuma, T. *Adv. Mater.* **2010**, *22*, 3185−3188.
(10) Kogo, A.; Sakai, N.; Tatsuma, T. *Nanoscale* **2012**, *4*, 4217−4221.
(11) Chen, Y.-S.; Choi, H.; Kamat, P. V. *J. Am. Chem. Soc.* **2013**, *135*, 8822−8825.
(12) Sakai, N.; Nakamura, S.; Tatsuma, T. *Dalton Trans.* **2013**, *42*, 16162−16165.
(13) Robel, I.; Kuno, M.; Kamat, P. V. *J. Am. Chem. Soc.* **2007**, *129*, 4136−4137.
(14) Kongkanand, A.; Tvrdy, K.; Takechi, K.; Kuno, M.; Kamat, P. V. *J. Am. Chem. Soc.* **2008**, *130*, 4007−4015.
(15) Bang, J. H.; Kamat, P. V. *ACS Nano* **2011**, *5*, 9421−9427.
(16) Zhao, K.; Pan, Z.; Mora-Seró, I.; Cánovas, E.; Wang, H.; Song, Y.; Gong, X.; Wang, J.; Bonn, M.; Bisquert, J.; Zhong, X. *J. Am. Chem. Soc.* **2015**, *137*, 5602−5609.
(17) Choi, H. M.; Ji, I. A.; Bang, J. H. *ACS Appl. Mater. Interfaces* **2014**, *6*, 2335−2343.
(18) Wang, J.; Mora-Seró, I.; Pan, Z.; Zhao, K.; Zhang, H.; Feng, Y.; Yang, G.; Zhong, X.; Bisquert, J. *J. Am. Chem. Soc.* **2013**, *135*, 15913−15922.
(19) Pan, Z.; Mora-Seró, I.; Shen, Q.; Zhang, H.; Li, Y.; Zhao, K.; Wang, J.; Zhong, X.; Bisquert, J. *J. Am. Chem. Soc.* **2014**, *136*, 9203−9210.
(20) Kim, C. S.; Choi, S. H.; Bang, J. H. *ACS Appl. Mater. Interfaces* **2014**, *6*, 22078−22087.
(21) Yu, Y.; Chen, X.; Yao, Q.; Yu, Y.; Yan, N.; Xie, J. *Chem. Mater.* **2013**, *25*, 946−952.
(22) Stamplecoskie, K. G.; Kamat, P. V. *J. Am. Chem. Soc.* **2014**, *136*, 11093−11099.
(23) Lee, E. J.; Nam, I.; Yi, J.; Bang, J. H. *J. Mater. Chem. A* **2015**, *3*, 3500−3510.
(24) Nosaka, A. Y.; Tanaka, G.; Nosaka, Y. *J. Phys. Chem. B* **2012**, *116*, 11098−11102.
(25) Rabenstein, D. L. *J. Am. Chem. Soc.* **1973**, *95*, 2797−2803.
(26) Feldt, S. M.; Gibson, E. A.; Gabrielsson, E.; Sun, L.; Boschloo, G.; Hagfeldt, A. *J. Am. Chem. Soc.* **2010**, *132*, 16714−16724.
(27) Lee, C.; Yang, W.; Parr, R. G. *Phys. Rev. B: Condens. Matter Mater. Phys.* **1988**, *37*, 785−789.
(28) Francl, M. M.; Pietro, W. J.; Hehre, W. J.; Binkley, J. S.; Gordon, M. S.; DeFrees, D. J.; Pople, J. A. *J. Chem. Phys.* **1982**, *77*, 3654−3665.
(29) Hariharan, P. C.; Pople, J. A. *Theoret. Chim. Acta* **1973**, *28*, 213−222.
(30) Hehre, W. J.; Ditchfield, R.; Pople, J. A. *J. Chem. Phys.* **1972**, *56*, 2257−2261.
(31) Hay, P. J.; Wadt, W. R. *J. Chem. Phys.* **1985**, *82*, 270−283.
(32) Runge, E.; Gross, E. K. U. *Phys. Rev. Lett.* **1984**, *52*, 997−1000.
(33) Ordejón, P.; Artacho, E.; Soler, J. M. *Phys. Rev. B: Condens. Matter Mater. Phys.* **1996**, *53*, R10441−R10444.
(34) Sánchez-Portal, D.; Ordejón, P.; Artacho, E.; Soler, J. M. *Int. J. Quantum Chem.* **1997**, *65*, 453−461.
(35) José, M. S.; Emilio, A.; Julian, D. G.; Alberto, G.; Javier, J.; Pablo, O.; Daniel, S.-P. *J. Phys.: Condens. Matter* **2002**, *14*, 2745.
(36) Troullier, N.; Martins, J. L. *Phys. Rev. B: Condens. Matter Mater. Phys.* **1991**, *43*, 1993−2006.
(37) Kleinman, L.; Bylander, D. M. *Phys. Rev. Lett.* **1982**, *48*, 1425−1428.
(38) Bylander, D. M.; Kleinman, L. *Phys. Rev. B: Condens. Matter Mater. Phys.* **1990**, *41*, 907−912.
(39) Perdew, J. P.; Burke, K.; Ernzerhof, M. *Phys. Rev. Lett.* **1996**, *77*, 3865−3868.
(40) Monkhorst, H. J.; Pack, J. D. *Phys. Rev. B* **1976**, *13*, 5188−5192.
(41) Wu, Z.; Jin, R. *Nano Lett.* **2010**, *10*, 2568−2573.
(42) Yu, Y.; Luo, Z.; Chevrier, D. M.; Leong, D. T.; Zhang, P.; Jiang, D.-e.; Xie, J. *J. Am. Chem. Soc.* **2014**, *136*, 1246−1249.
(43) Stamplecoskie, K. G.; Chen, Y.-S.; Kamat, P. V. *J. Phys. Chem. C* **2013**, *118*, 1370−1376.
(44) Chung, I.; Lee, B.; He, J.; Chang, R. P. H.; Kanatzidis, M. G. *Nature* **2012**, *485*, 486−489.
(45) Feldt, S. M.; Wang, G.; Boschloo, G.; Hagfeldt, A. *J. Phys. Chem. C* **2011**, *115*, 21500−21507.
(46) González-Pedro, V.; Xu, X.; Mora-Seró, I.; Bisquert, J. *ACS Nano* **2010**, *4*, 5783−5790.
(47) Bisquert, J.; Fabregat-Santiago, F.; Mora-Seró, I.; Garcia-Belmonte, G.; Giménez, S. *J. Phys. Chem. C* **2009**, *113*, 17278−17290.
(48) Fabregat-Santiago, F.; Bisquert, J.; Garcia-Belmonte, G.; Boschloo, G.; Hagfeldt, A. *Sol. Energy Mater. Sol. Cells* **2005**, *87*, 117−131.
(49) Bisquert, J.; Garcia-Belmonte, G.; Bueno, P.; Longo, E.; Bulhões, L. O. S. *J. Electroanal. Chem.* **1998**, *452*, 229−234.
(50) Barea, E. M.; Shalom, M.; Giménez, S.; Hod, I.; Mora-Seró, I.; Zaban, A.; Bisquert, J. *J. Am. Chem. Soc.* **2010**, *132*, 6834−6839.
(51) Shalom, M.; Rühle, S.; Hod, I.; Yahav, S.; Zaban, A. *J. Am. Chem. Soc.* **2009**, *131*, 9876−9877.
(52) Basit, M. A.; Abbas, M. A.; Bang, J. H.; Park, T. J. *J. Alloys Compd.* **2015**, *653*, 228−233.
(53) Abbas, M. A.; Basit, M. A.; Park, T. J.; Bang, J. H. *Phys. Chem. Chem. Phys.* **2015**, *17*, 9752−9760.
(54) Lan, J.-L.; Wei, T.-C.; Feng, S.-P.; Wan, C.-C.; Cao, G. *J. Phys. Chem. C* **2012**, *116*, 25727−25733.
(55) Urbani, M.; Grätzel, M.; Nazeeruddin, M. K.; Torres, T. *Chem. Rev.* **2014**, *114*, 12330−12396.
(56) Luque, A.; Hegedus, S. *Handbook of Photovoltaic Science and Engineering*; John Wiley and Sons, Ltd.: New York, 2011.
(57) Bisquert, J.; Mora-Seró, I. *J. Phys. Chem. Lett.* **2010**, *1*, 450−456.
(58) Leng, W. H.; Barnes, P. R. F.; Juozapavicius, M.; O'Regan, B. C.; Durrant, J. R. *J. Phys. Chem. Lett.* **2010**, *1*, 967−972.
(59) Peter, L. *Acc. Chem. Res.* **2009**, *42*, 1839−1847.
(60) James, R. J.; Feng, L.; Qing, W. *J. Phys. Chem. C* **2010**, *114*, 14665−14674.
(61) Jing, B.; Zhang, H.; Zhang, M.; Lu, Z.; Shen, T. *J. Mater. Chem.* **1998**, *8*, 2055−2060.
(62) Janne, H.; Gerrit, B.; Anders, H.; Peter, L. *J. Phys. Chem. C* **2008**, *112*, 5623−5637.
(63) Bertoluzzi, L.; Ma, S. *Phys. Chem. Chem. Phys.* **2013**, *15*, 4283−4285.
(64) Tvrdy, K.; Frantsuzov, P. A.; Kamat, P. V. *Proc. Natl. Acad. Sci. U. S. A.* **2011**, *108*, 29−34.
(65) Hara, K.; Sato, T.; Katoh, R.; Furube, A.; Ohga, Y.; Shinpo, A.; Suga, S.; Sayama, K.; Sugihara, H.; Arakawa, H. *J. Phys. Chem. B* **2003**, *107*, 597−606.
(66) Koops, S. E.; O'Regan, B. C.; Barnes, P. R. F.; Durrant, J. R. *J. Am. Chem. Soc.* **2009**, *131*, 4808−4818.
(67) Hagfeldt, A.; Grätzel, M. *Acc. Chem. Res.* **2000**, *33*, 269−277.
(68) Snaith, H. J. *Adv. Funct. Mater.* **2010**, *20*, 13−19.
(69) Hardin, B. E.; Snaith, H. J.; McGehee, M. D. *Nat. Photonics* **2012**, *6*, 162−169.
(70) Clifford, J. N.; Palomares, E.; Nazeeruddin, M. K.; Gratzel, M.; Durrant, J. R. *J. Phys. Chem. C* **2007**, *111*, 6561−6567.
(71) Boschloo, G.; Hagfeldt, A. *Acc. Chem. Res.* **2009**, *42*, 1819−1826.
(72) DeVries, M. J.; Pellin, M. J.; Hupp, J. T. *Langmuir* **2010**, *26*, 9082−9087.
(73) Hodes, G. *J. Phys. Chem. C* **2008**, *112*, 17778−17787.
(74) Aribia, K. B.; Moehl, T.; Zakeeruddin, S. M.; Grätzel, M. *Chem. Sci.* **2013**, *4*, 454−459.
(75) Nusbaumer, H.; Zakeeruddin, S. M.; Moser, J. E.; Grätzel, M. *Chem. - Eur. J.* **2003**, *9*, 3756−3763.
(76) Kashif, M. K.; Axelson, J. C.; Duffy, N. W.; Forsyth, C. M.; Chang, C. J.; Long, J. R.; Spiccia, L.; Bach, U. *J. Am. Chem. Soc.* **2012**, *134*, 16646−16653.
(77) Yum, J. H.; Baranoff, E.; Kessler, F.; Moehl, T.; Ahmad, S.; Bessho, T.; Marchioro, A.; Ghadiri, E.; Moser, J. E.; Yi, C.; Nazeeruddin, M. K.; Grätzel, M. *Nat. Commun.* **2012**, *3*, 631.
(78) Wang, M.; Chen, P.; Humphry-Baker, R.; Zakeeruddin, S. M.; Grätzel, M. *ChemPhysChem* **2009**, *10*, 290−299.

DOI: 10.1021/jacs.5b11174
J. Am. Chem. Soc. 2016, 138, 390−401

(79) Klahr, B. M.; Hamann, T. W. *J. Phys. Chem. C* **2009**, *113*, 14040−14045.
(80) Nelson, J. J.; Amick, T. J.; Elliott, C. M. *J. Phys. Chem. C* **2008**, *112*, 18255−18263.
(81) Mosconi, E.; Yum, J.-H.; Kessler, F.; Gómez García, C. J.; Zuccaccia, C.; Cinti, A.; Nazeeruddin, M. K.; Grätzel, M.; De Angelis, F. *J. Am. Chem. Soc.* **2012**, *134*, 19438−19453.
(82) Feldt, S. M.; Lohse, P. W.; Kessler, F.; Nazeeruddin, M. K.; Grätzel, M.; Boschloo, G.; Hagfeldt, A. *Phys. Chem. Chem. Phys.* **2013**, *15*, 7087−7097.
(83) Zaban, A.; Greenshtein, M.; Bisquert, J. *ChemPhysChem* **2003**, *4*, 859−864.
(84) Kim, H.-S.; Lee, C.-R.; Im, J.-H.; Lee, K.-B.; Moehl, T.; Marchioro, A.; Moon, S.-J.; Humphry-Baker, R.; Yum, J.-H.; Moser, J. E.; Grätzel, M.; Park, N.-G. *Sci. Rep.* **2012**, *2*, 591.

DOI: 10.1021/jacs.5b11174
J. Am. Chem. Soc. 2016, 138, 390−401